Hydrology and
Earth System
Sciences
Discussions

Vegetation Greening Significantly Reduced the Capacity of Water Supply to China's South-North Water Diversion Project

Jiehao Zhang[1,2], Yulong Zhang[3], Ge Sun[4], Conghe Song[2], Matthew P. Dannenberg[5], Jiangfeng Li[1], Ning Liu[4], Kerong Zhang[6], Quanfa Zhang[6]

5 [1]Department of Land Management, China University of Geosciences, Wuhan, 430074, China.
[2]Department of Geography, University of North Carolina at Chapel Hill, Chapel Hill, NC 27599, USA.
[3]Institute for a Secure and Sustainable Environment, University of Tennessee, Knoxville, TN 37902, USA.
[4]Eastern Forest Environmental Threat Assessment Center, USDA Forest Service, Research Triangle Park, NC 27709, USA.
[5]Department of Geographical and Sustainability Sciences, University of Iowa, Iowa City, IA 52242, USA.
10 [6]Wuhan Botanical Garden, Chinese Academy of Sciences, Wuhan, 430074, China.

Corresponding to: Jiehao Zhang (zhangjiehao1993@gmail.com); Conghe Song (csong@email.unc.edu)

Abstract. Recent climate change and vegetation greening have important implications to Earth's global biogeochemical cycles and climate, raising concerns about the water supply for large water diversion projects. To quantify the greening impacts on local water balance and the capacity of water supply, we built a hybrid model based on the Coupled Carbon and Water (CCW) and Water Supply Stress Index (WaSSI) models and conducted a case study on the Upper Han River Basin (UHRB) in central China that serves as the water source area to the middle route of the South-North Water Diversion Project (SNWDP). Significant vegetation greening occurred in the UHRB during 2001-2018, with the normalized difference vegetation index increasing at a rate of 0.5% yr^{-1} (p < 0.01) but no significant trends in climate during the same period (albeit with large interannual climate variability). Annual water yield (WY) greatly decreased during this period, and vegetation greening alone induced a significant WY decrease of 3.5 mm yr^{-1} (p < 0.01). Vegetation greening could potentially reduce the annual water supply by 7.3 km^3 on average, accounting for 77% of the intended annual water diversion volume of SNWDP. Vegetation greening could also increase the possibility of hydrological drought and reduce about a quarter of WY on average during drought periods. In the future, water supply capacity is likely to decline further as vegetation greening continues along with increasing temperature and vapor pressure deficit. Our findings demonstrate the large effects of vegetation greening on water balance and hydrological drought, which have important implications for management of water resources in long-range water diversion projects.

1 Introduction

As the world's population and economy expand under a changing climate, human demand for freshwater increases and water shortage has become a concern globally (Jackson et al., 2001). Water diversion with long-range transport is an effective way

30 to alleviate regional water shortage (Emanuel et al., 2015). However, the sustainability of such projects depends on water

supply from the donor watersheds, which is uncertain due to environmental change. For example, recent the land 'greening up' that may affect the watershed balance and thus the hydrological services. Vegetation greening has been observed globally as a result of the rapid changing climate and land cover (Chen et al., 2019; Guay et al., 2014; Zhang et al., 2017; Zhu et al., 2013), exerting great uncertainties on water availability in source regions of water diversion projects. A better

35   understanding of the hydrological effects of vegetation greening on water supply of water diversion projects is critical for watershed management to mitigate the influences of climate change and human activities (van Loon et al., 2016).

The South to North Water Diversion Project (SNWDP) is the largest hydrological engineering project (in terms of investment) in the world to mitigate the water shortage in North China (Zhang, 2009). The Upper Han River Basin (UHRB), a subtropical basin in central China, is the water source area for the middle route of the SNWDP. The planned total water diversion each

40   year during Phase I of the middle route project is 9.5 km^3, accounting for about one-third of the mean annual runoff of the UHRB. However, water yield in the UHRB has sharply declined since the early 1990s (Chen et al., 2007; Liu et al., 2012; She et al., 2017). Moreover, the UHRB is susceptible to frequent hydrological droughts (Xu et al., 2011; Zhang et al., 2018) because about 70% of its precipitation is recycled back to the atmosphere via evapotranspiration (ET) (China Meteorological Administration, 2019). The capacity of water supply to the SNWDP in drought years can be half of that of a normal year

45   (Wang and Yang, 2005), exerting a large influence on the water supply capacity of the water diversion project, especially at the seasonal scale. The drought risks are likely compounded by warming-induced increases in the evaporative demand due to the rise of the vapor pressure deficit (Cook et al., 2014, 2020; Lesk et al., 2016; Williams et al., 2020). These conditions raised concerns about the extent to which water yield of the UHRB can meet expectations for the SNWDP.

The afforestation led vegetation greening in the UHRB also exerted uncertainties on the water availability. Considering the

50   importance of the UHRB for the SNWDP, China implemented large-scale afforestation and ecological restoration projects to safeguard water availability and quality from the UHRB. The afforestation-driven greening of the UHRB has been larger and more significant than in most other parts of the world (Chen et al., 2019). The greening of the UHRB could create a trade-off between ecological restoration and water availability (Jackson et al., 2005). The increased forest cover in the UHRB could reduce sediment in the streamflow and improve water quality (Li et al., 2008; Piégay et al., 2004; Soutar, 1989). However, this

55   rapid vegetation change could exert considerable influences on the water cycle (Bai et al., 2019; Li et al., 2018), thus directly altering the capacity of water supply to the SNWDP. Specifically, greater leaf area and enhanced vegetation activity potentially consumes more water through transpiration, which could lead to a reduction in water yield (Bai et al., 2020; Cao et al., 2016; Li et al., 2018), especially during drought periods (Teuling et al., 2013; Tian et al., 2018). How this rapid and widespread greening has affected water yield in the UHRB, thus the water supply to the middle route SNWDP, remains largely unknown.

60   Paired-watershed experiments, one of the most effective and intuitive methods to investigate the mechanisms of changes in water balance (Wei et al., 2008), is not feasible at a large spatial scale. Eco-hydrological models based on remote sensing inputs provide an efficient way to understand hydrological processes at a high spatial resolution over large areas and long time periods (Wang and Dickinson, 2012). To investigate interactions among vegetation, climate, and the water cycle in the UHRB,

a model simulating hydrological variables should consider the effects of both vegetation and climate change based on a

65 mechanistic, process-based understanding of hydrology. While many studies have investigated hydrological processes using mechanistic land surface models (Baker and Miller, 2013; Shin et al., 2019; Xi et al., 2018), their complex model structures and a large number of parameters limit their applicability at a large spatial scale. Likewise, carbon and water fluxes of vegetation are tightly connected, but many hydrological models lack biological constraints of photosynthetic carbon uptake in quantifying hydrological entities.

70 To navigate this trade-off between mechanistic carbon-water linkage and computational efficiency, we developed and applied a new hybrid model that integrates two existing models: the 'water centric' Water Supply Stress Index (WaSSI) model (Caldwell et al., 2012; Liu et al., 2020; Sun et al., 2016) and the 'carbon centric' Coupled Carbon and Water (CCW) model (Zhang et al., 2016, 2019b). Here, we use this coupled model to address the following questions: 1) What were the spatial and temporal patterns of annual and monthly water yield (WY) in the UHRB from 2001 to 2018? 2) To what extent did the rapid

75 vegetation greening affect WY in the UHRB and thus water supply for the SNWDP? 3) How did vegetation greening alter hydrological drought regimes in the UHRB? Overall, our goal is to improve understanding of the effects of vegetation greening on the water balance and hydrological drought and to provide a scientific basis for managing watersheds that serve as critical water supply in inter-basin transfers projects.

2 Methods and data

80 ### 2.1 Study area

The Han River in central China covers approximately 1.59×10^5 km^2 with a total length of 1,577 km (Jin and Guo, 1993; Yang et al., 1997), making it the longest tributary of the Yangtze River. Its mountainous upper reaches (31°20'–34°10' N, 106°–112° E; 210 – 3,500 m a.s.l) are 925 km long and drain an area of approximately 9.5×10^4 km^2 (Yang et al., 1997). The historical mean annual runoff of the UHRB is 41.1 km^3 (though with high interannual variability) (Yang et al., 1997). The Danjiangkou

85 Reservoir, located in the easternmost tip of the UHRB, stores runoff from the UHRB and serves as the water source for the middle route of the SNWDP (Figure 1).
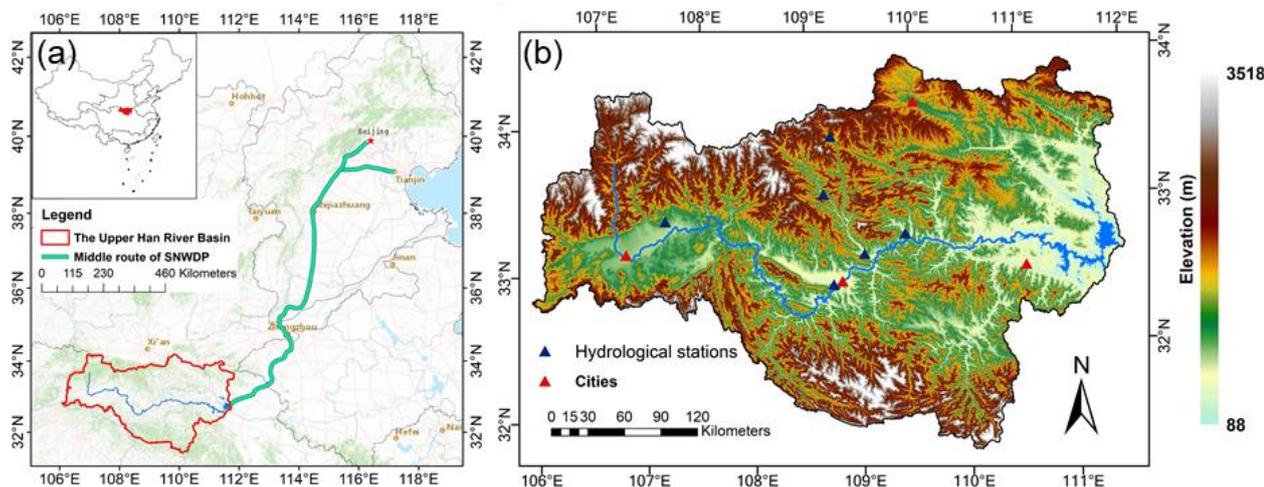
Figure 1: (a) The location of the UHRB in China and the middle route of the South-North Water Diversion Project (from the Map World); (b) Topography of the UHRB, where the red triangles mark the location of the major cities and the black triangles signifies
90   **hydrological stations, whose data will be used for our model evaluation.**

The SNWDP is an ambitious plan to alleviate the water shortage in North China, whose water consumption and requirements have increased greatly since the 1980s due to the increasing acceleration of both economic development and population growth (Liu and Zheng, 2002). The SNWDP serves roughly 400 million people, accounting for about one-third of China's population. However, annual available water resources per capita in North China are less than one-quarter of those of South China (Zhang

95   et al., 2020). Water shortages in North China, including the capital, Beijing, have become a major factor constraining economic and social development. The SNWDP consists of three routes: the eastern, the middle, and the western routes (Liu and Zheng, 2002). The eastern route follows through the course of an ancient canal in East China to divert water from the lower Yangtze River, the middle route from the UHRB via aqueducts, and the western route from the upper Yangtze River (in the planning stage) (Liu and Zheng, 2002).

100   **2.2 Data Sources and Processing**

The land cover and vegetation index data used in this study were obtained from the Moderate Resolution Imaging Spectroradiometer (MODIS) data products (Table 1). We obtained the land cover data for 2001-2018 from the MODIS annual 500m land cover product (MCD12Q1 v006), using the International Geosphere-Biosphere Programme (IGBP) classification scheme (Sulla-Menashe et al., 2019). We also obtained 16-day, 250m monthly normalized difference vegetation index (NDVI)

105   from the MODIS MOD13Q1 v006 product for the same period (Huete et al., 2002), which we smoothed with the adaptive Savitzky-Golay filter in the TIMESAT 3.3 software (Jönsson and Eklundh, 2004) then aggregated to monthly scale with temporal averaging.

4

The climate data used to drive the model included precipitation (P), air temperature (T), vapor pressure deficit (VPD, in hPa), and shortwave radiation (SR), which were all obtained from the monthly, ~4 km (1/24 degree) TerraClimate dataset

110 (Abatzoglou et al., 2018) for 2001 to 2018 (Table 1). We estimated the mean temperature by averaging monthly maximum and minimum temperature.

Soil attributes were derived from the SoilGrids dataset (Table 1), a system for global digital soil mapping using a state-of-the-art machine learning method to map the spatial distribution of soil properties across the globe. SoilGrids prediction models are fitted using over 230,000 soil profile observations from the World Soil Information Service database and a series of

115 environmental covariates. The soil data we used to drive the model included sand, silt, and clay content at six standard depth intervals at a spatial resolution of 250 meters. All spatial data were rescaled to 250m resolution based on the cubic convolution resampling method in ArcGIS 10.5, except the land cover data which was resampled based on the nearest neighbour.

Table 1: *The Data Sources and Intended Usage in This Study*. **Note: The climate data include precipitation, air temperature, vapor pressure deficit, and shortwave radiation at monthly time steps.**

Dataset	Source	Usage	Spatial and Temporal Resolution	Period
Digital elevation model	Shuttle Radar Topography Mission (SRTM)	Drive CCW model & Extract Watersheds	30m/~	~
Land cover	MODIS, MCD12Q1 v006	Drive CCW model	500m/Yearly	2001~2018
NDVI	MODIS, MOD13Q1 v006	Drive CCW model	250m/16-day	2001~2018
Climate	TerraClimate*	Drive CCW and WaSSI	4km/Monthly	2001~2018
Soil	SoilGrids from the International Soil Reference and Information Centre	Drive WaSSI	250m/~	~
Measured streamflow	Records of the hydrological gauging stations	Model evaluation	~/Monthly or yearly	2009~2015

120 * **http://www.climatologylab.org/terraclimate.html**

2.3 Model development

We integrated the WaSSI model (Sun et al. 2011) and the CCW model (Zhang et al., 2016) and called it as CCW-WaSSI model. We used the remote sensing-based, data-driven ET model from CCW as input to the WY model from WaSSI (Figure 2). The 'water centric' WaSSI model is an integrated ecohydrological model designed for modeling water balance and carbon

125 assimilation at a broad scale. The essential components of WaSSI include an empirical ET model and a soil water routing model for estimating ET, water yield, and ecosystem productivity (Caldwell et al., 2012; Sun et al., 2011, 2015). Due to the lack of representation of biophysical processes in modeling ET in WaSSI, we replaced it with the carbon-centric ET model from CCW, which effectively couples the carbon assimilation (gross primary production, GPP) and ET processes at the

Hydrology and
Earth System
Sciences
Discussions
Open Access

EGU

130   monthly scale (Zhang et al., 2016). As a result, the hybrid model retains mechanistic linkages between carbon and water in the CCW model and the simplicity and computational efficiency of both models. The original WaSSI and CCW are written in FORTRAN and Interactive Data Language, respectively. Here we re-wrote the integrated model with Python 3.8.

CCW has a much simpler model structure than the more complex process-based models for ET while maintaining similar accuracy (Zhang et al., 2016, 2019b). Driven by remotely sensed data, CCW first estimates GPP based on light-use-efficiency (LUE) theory (Figure 2), from which ET is estimated based on underlying water-use efficiency (UWUE) theory (Zhou et al.,
135   2014):

$$GPP = APAR \times \varepsilon = (PAR \times FPAR) \times \left(\varepsilon_{pot} \times R_s\right) \times (T_s \times W_s), \qquad (1)$$

$$ET = \frac{GPP \times VPD^k}{UWUE}, \qquad (2)$$

where APAR is the absorbed photosynthetically active radiation (MJ m^{-2}), which is assumed to be 45% of the total shortwave radiation (Running et al., 2000); FPAR is the fraction of photosynthetically active radiation (PAR) absorbed by plants; ε_{pot}
140   (g·C MJ^{-1}) is the potential LUE under optimal conditions; R_s, T_s, and W_s are, respectively, environmental scalars (in the range of [0,1]) related to diffuse radiation, temperature, and moisture stresses to primary production; UWUE represents the biome-specific underlying water use efficiency, derived from global flux tower data (Pastorello et al., 2020), ranging from 4.5 to 8.4 g C/kg H$_2$O for different land cover types; and k is an empirical parameter set to 0.5. CCW was calibrated and comprehensively validated based on global FLUXNET data (Zhang et al., 2016, 2019b).

145   Using ET estimated from CCW, we estimated WY with WaSSI (Figure 2). The Sacramento Soil Moisture Accounting Model (SAC-SMA) (Burnash, 1995; Burnash et al., 1973) was used to model WY in the WaSSI model, driven by ET, precipitation (P), and soil attributes. The algorithm divides the soil layer into lower and upper zones at different depths and estimates the distribution of moisture—including both tension water components (driven by evapotranspiration and diffusion) and free water components (driven by gravitational forces) in each of these two zones (Figure 2). The model then uses P, soil moisture, and
150   the basin's relative permeability to estimate total water storage and run-off (Figure 2).
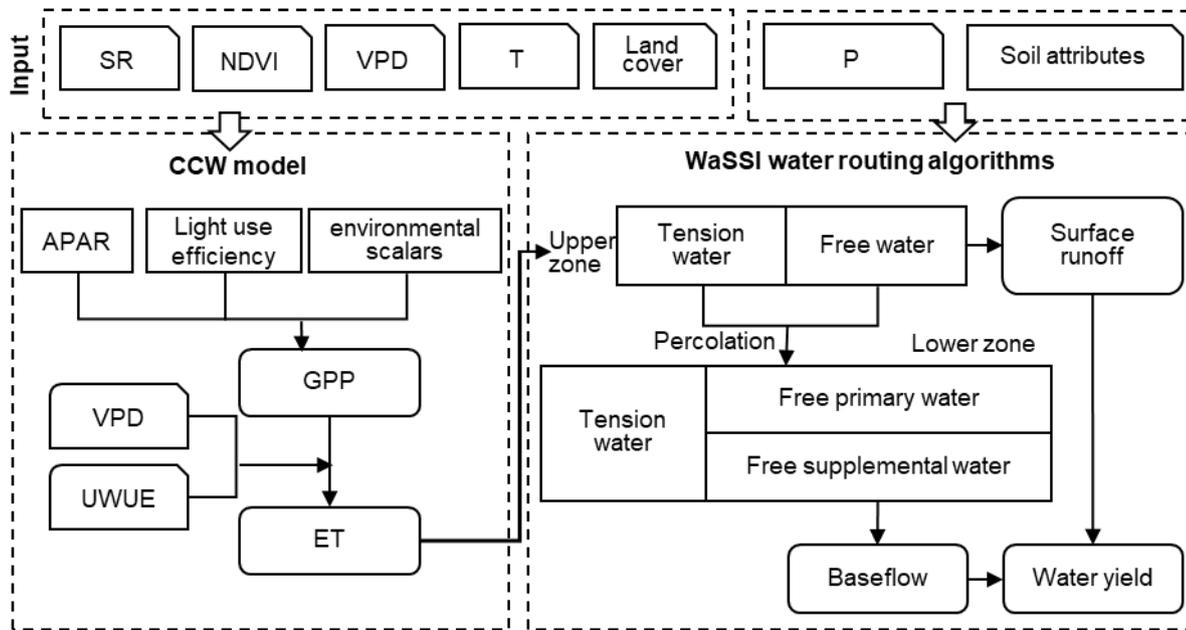
Figure 2: The framework of the CCW-WaSSI hybrid ecohydrology model, CCW-WaSSI. The corner-snipped rectangles denote inputs of the model, the rectangles denote processes of the model, and the rounded rectangles denote outputs of the model. Arrows show the model process direction.

155

2.4 Model Evaluation

To evaluate the performance of the CCW-WaSSI model, we compared the estimated WY to the measured streamflow of the hydrological gauging stations within the UHRB. First, we used the six stations within the basin that were relatively free from direct human modification (e.g., hydropower plants, reservoirs, dams) (Figure 1b) to evaluate the model both at monthly and annual scale. Then we used the records of annual streamflow to the Danjiangkou Reservoir to evaluate the modeled WY for the overall UHRB. It should be noted that the streamflow records of Reservoir were under the influences of at least four major hydropower plants along the Han River mainstream and countless other hydraulic engineering within the UHRB. We used the Nash-Sutcliffe efficiency (NSE) and the coefficient of determination (R^2) to compare modeled WY with the observed WY. The NSE is a widely used, reliable statistic for assessing the goodness of fit of hydrologic models, calculated as one minus the ratio of the error variance of the modeled time-series divided by the variance of the observed time-series (McCuen et al., 2006).

2.5 Model simulations of greening effects on water yield

To explore the relative contributions of vegetation and climate on WY, we designed three scenario experiments (Table 2). We first simulated the actual variation of WY based on dynamic land cover type, NDVI, and climate from 2001 to 2018 (Scenario S1), thus representing the combined effects from both climate and vegetation. To isolate the effect of vegetation alone on WY,

7

170   we designed two more simulation scenarios. In Scenario S2, we fixed land cover and NDVI in 2001, while all climatic variables were allowed to change, thus obtaining climate effects on WY without any vegetation greening. In Scenario S3, we fix land cover and NDVI in 2018 and allow the climatic variable to change with time, thus simulating WY after vegetation greening. We then estimated two types of greening effects on WY using a difference-in-difference approach: the dynamics greening effects (S1−S2) and potential greening effects (S3−S2). The dynamic greening effects are the dynamic WY changes caused

175   by vegetation greening alone during 2001-2018. The potential greening effects are the differences in WY between S2 and S3, which is the possible changes in WY from vegetation greening during 2001-2018 if each year had the same vegetation greening condition in 2018. Unlike dynamic greening effects, the potential greening effects can present a range of greening effects with the variation of climate conditions, which is expected to continue in the future. To investigate trends in WY for each scenario, we used the Mann-Kendall test, a widely used test in hydrological studies for trend and change point detection (Hamed, 2008).

180   To quantify changes in hydrological drought risk from vegetation greening, we calculated a hydrological drought index from WY under the three scenarios. Hydrological drought refers to a severe lack of water in the hydrological system, manifesting in abnormally low streamflow in rivers and abnormally low water levels in lakes, reservoirs, and groundwater (van Loon, 2015). Here, the monthly drought index was calculated as the percentages of monthly WY to the mean WY of the same month during 2001-2018 (Hayes et al., 2002). We then classified drought intensities for each month based on the magnitude of the

185   drought index. Specifically, months with WY within 10% above or below average were classified as "normal"; months with WY 10%-30% above or below average were classified as "moderate drought/wet"; months with WY 30%-50% above or below average were classified as "severe drought/wet"; and months with WY greater than 50% above or below average were classified as "extreme drought/wet".

Table 2: Variable settings and purposes of modelling scenarios.

Scenarios	NDVI and land cover	Climate variables	Purposes
S1	Dynamic	Dynamic	Estimating actual dynamics of water yield
S2	Fixed in 2001	Dynamic	Estimating possible water yield without vegetation greening
S3	Fixed in 2018	Dynamic	Estimating possible water yield after vegetation greening

190

8

3 Results

3.1 Vegetation and climate changes in the UHRB

The annual mean NDVI over the UHRB showed a significant upward trend with a rate of 0.5% yr^{-1} (p < 0.01) (Figure 3a).
Spatially, 97.4% of the area had increasing trends, 94.0% of which were statistically significant (p < 0.05). The few areas with
195 decreasing trends were distributed around the cities and the Danjiangkou Reservoir. In total, 17.9% of the land area in the
basin experienced a change in land cover between 2001 and 2018. Forest cover increased from 40.9% (38,753.6 km^2) in 2001
to 50.7% (48,012.6 km^2) in 2018 (Figure 3b), and 98.8% of the new increased forests were converted from shrubland.
Shrubland showed the largest decrease by 18.3%, from 51.8% (49,093.4 km^2) in 2001 to 42.3% (40,025.5 km^2) in 2018 (Figure
3b). The area of cropland decreased by 9.9% from 5,175.1 km^2 (5.5%) in 2001 to 4660.8 km^2 (4.9%) in 2018. The area covered
200 by open water more than doubled, from 313.1 km^2 in 2001 to 746.6 km^2 in 2018, likely caused by increasing water levels in
the Danjiangkou Reservoir for providing water to the SNWDP.

Due to high interannual variability and the relatively short study period (less than 20 years), none of the four climatic variables
(i.e., P, T, VPD, SR) showed statistically significant trends at the annual scale (Figure A1 in Appendix).
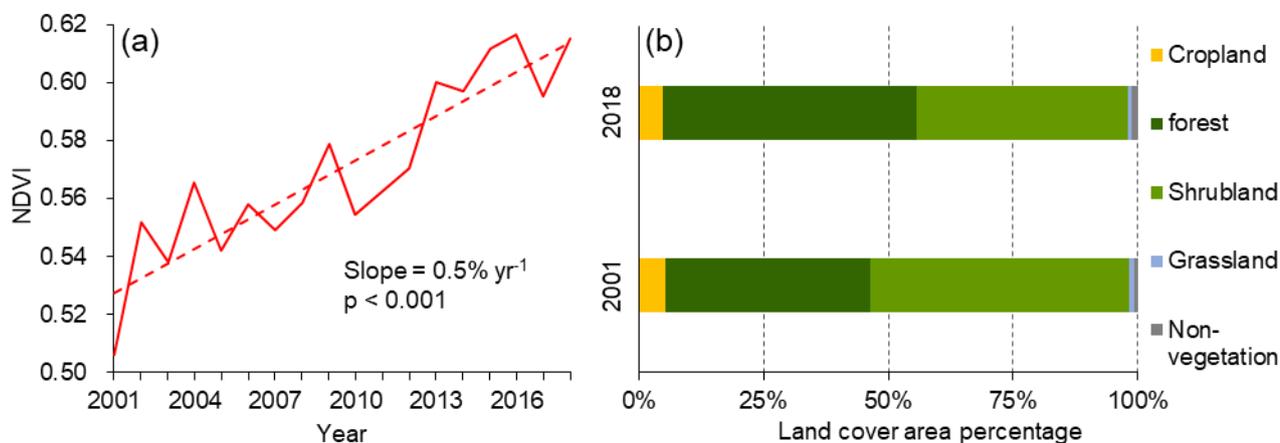
205 Figure 3: (a) The temporal variation of annual mean NDVI in the UHRB during 2001-2018; (b) The composition of the main land
cover types in the UHRB in 2001 and 2018.

3.2 Model evaluation

The CCW-WaSSI model performed well in estimating the annual and monthly WY at six hydrological gauging stations and
the overall UHRB. At the entire watershed scale, the CCW-WaSSI model captured 90% of annual WY variation (R^2 = 0.9),
210 with an NSE of 0.8, RMSE of 3.9 km^3 yr^{-1} (Figure 4a). At the sub-watershed scale with six hydrological gauging stations, the
model captured 80% of the annual WY variation (R^2 = 0.8), with an NSE of 0.9, RMSE of 96.3 mm yr^{-1} (Figure 4b). Monthly-
scale NSE across the six stations (Figure 4) ranged 0.5-0.8. The model captured 50%-80% of the monthly variation (R^2 = 0.5-

9

0.8) of WY, with root mean squared errors (RMSE) of 15.9-30.7 mm per month (Figure 4c). Averaged across all gauges, monthly NSE was 0.6, R^2 was 0.7, and RMSE was 21.2 mm per month.
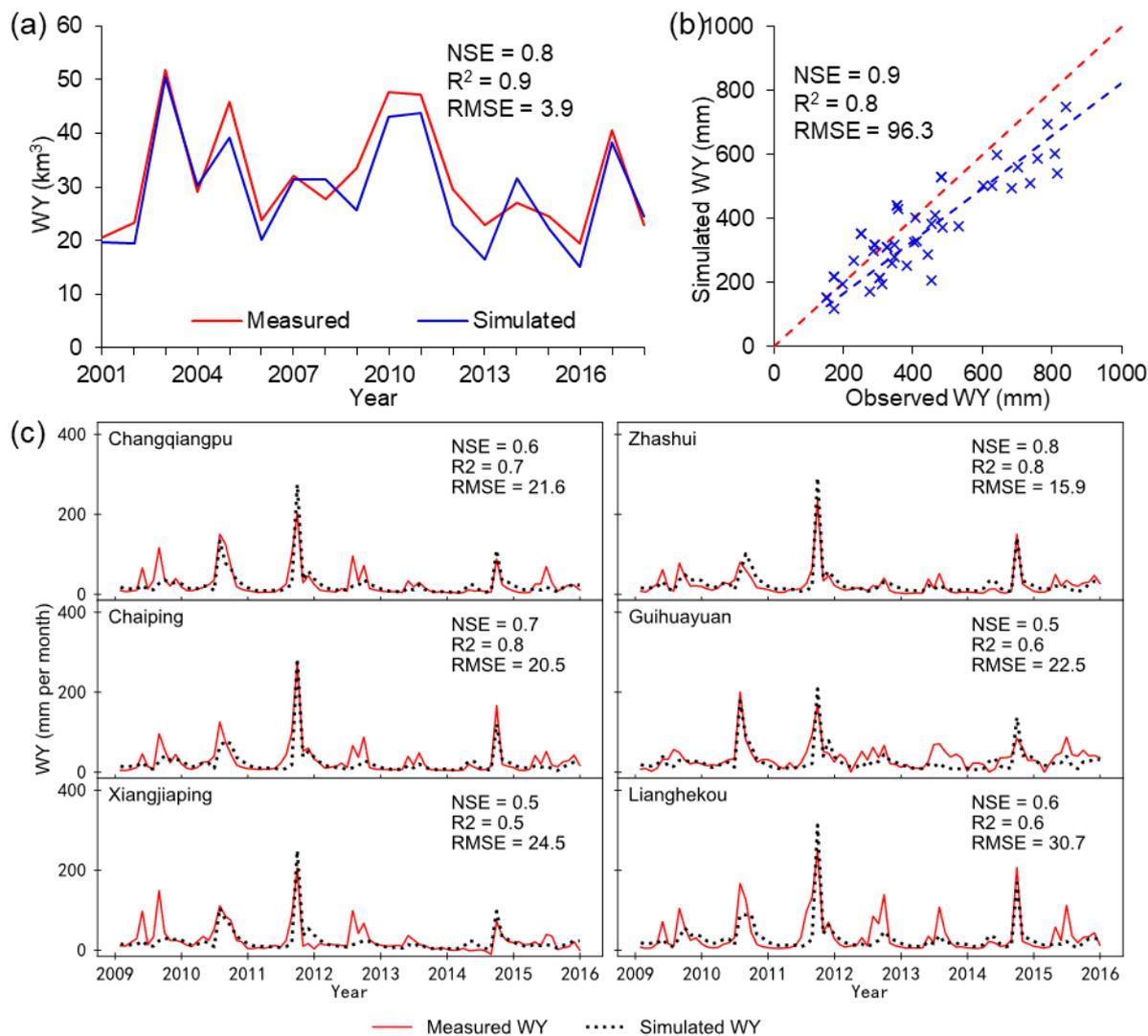
215

Figure 4: (a) Time series of the simulated water yield (WY) and measured streamflow to the Danjiangkou Reservoir at the annual scale; (b) Comparison between simulated and observed annual WY for six hydrological gauging stations within the UHRB, shown in Figure 1; (c) Time series of the simulated and measured WY at the monthly scale for six hydrological gauging stations.

Hydrology and
Earth System
Sciences
Discussions
Open Access

EGU

3.3 Changes in water yield (WY)

In scenario S1 (all factors), the UHRB had an annual WY of 205.4-533.3 mm yr^{-1}, with a mean of 308.5 mm yr^{-1} during 2001-2018 (Figure 5a, 5b), peaking in late summer to early autumn and accounting for 34% of the mean annual P (Figure 5d). The overall WY in the UHRB slightly decreased at a rate of -2.9 mm yr^{-1} over the study period, though this trend was not statistically significant (p = 0.58). Decreasing trends of WY occurred over 74% of the UHRB, though only 9% of the basin had a trend at the confidence level of 90% (p < 0.10; see Appendix Figure A3). Using the Mann-Kendall test, change points of annual WY were detected during 2009-2011 (Appendix Figure A2). The average annual WY before this change point (2001-2008, 319.3 mm yr^{-1}) was 60.8 mm higher than that after the change point (2012-2018, 258.5 mm) (Figure 5b). In contrast, the difference in the average annual P was only 24.1 mm between the two periods, so the difference in annual WY cannot be explained by precipitation alone.
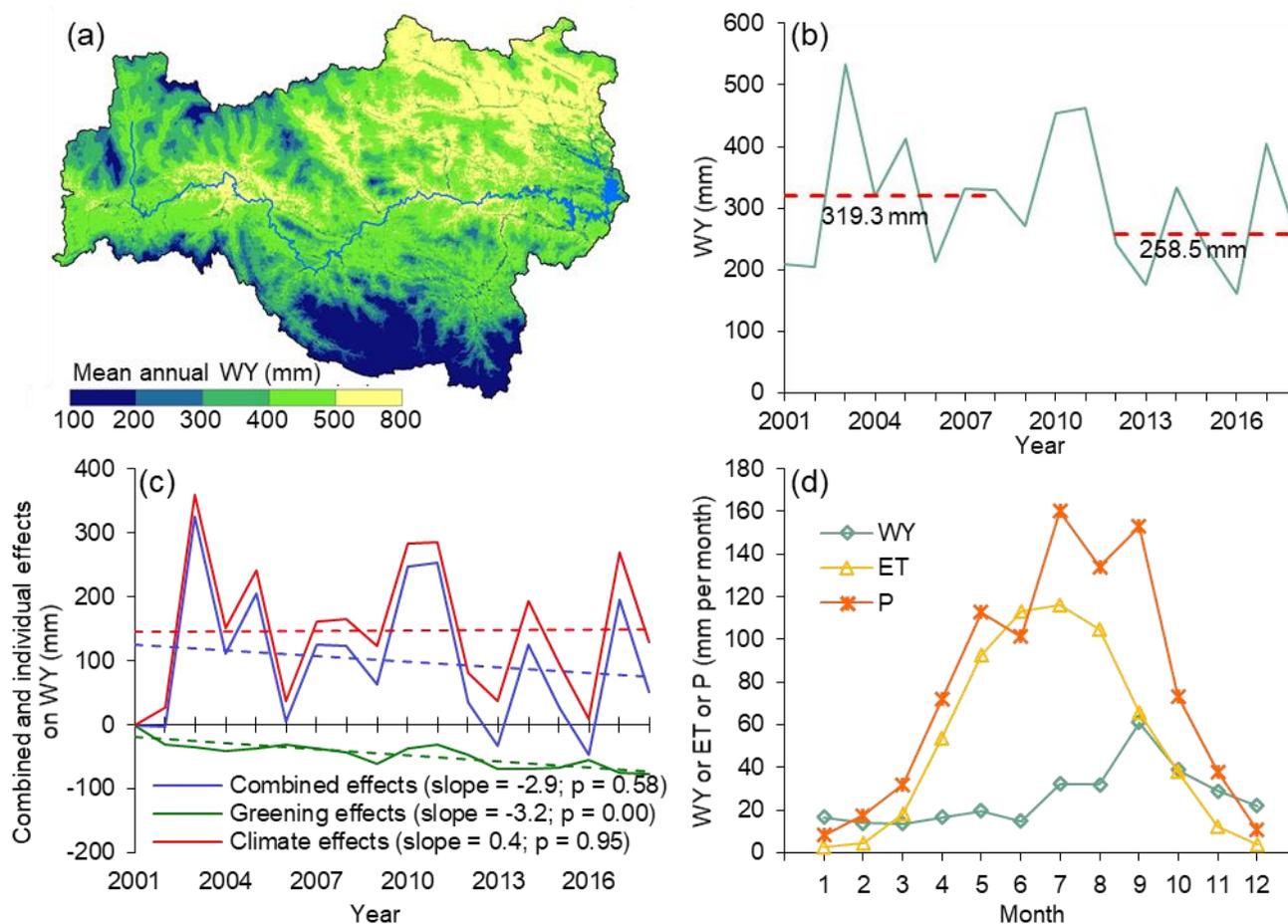
Figure 5: (a) The spatial distribution of mean annual water yield (WY) during 2001-2018 in the Upper Han River Basin; (b) The temporal variation of annual WY (Scenario S1) during 2001-2018, the dashed red lines denote the mean annual WY for periods

before (2001-2008) and after (2009-2018) Mann-Kendall change points; (c) The combined and individual effects of vegetation and climate on WY during 2001-2018; (d) Average monthly evapotranspiration (ET), WY, and precipitation (P) during 2001-2018.

235   The model experiments revealed that vegetation greening had a significant negative effect on annual WY with a rate of -3.2 mm yr^{-1} (p < 0.01) during 2001-2018 (Figure 5c). Spatially, greening induced a WY decrease in 90% of the UHRB, while WY increases due to greening were mainly in high elevation areas (above 3000m). The WY decrease from greening had strong negative correlation over space with elevation (R=-0.7), and positive correlation with average annual temperature (R=0.7) and VPD (P=0.8). The effects of climate on WY varied substantially from year-to-year, with a standard deviation (STD) of 101.9

240   mm, but had no significant trend (slope = 0.4 mm yr^{-1}; p = 0.95; Figure 5b). These climate effects were also the main driver of overall annual WY variation (STD = 108.6).

    In addition to reducing total WY, vegetation greening also significantly reduced the ratio of annual WY to P (Figure 6a). After the first change point of WY/P ratio identified by the Mann-Kendall method in 2003, the ratio decreased with a significant trend of 0.008 yr^{-1} (p = 0.06) (Figure 6a). The annual WY/P ratio also had a significant negative correlation with NDVI, with

245   a correlation coefficient of −0.7 (p = 0.00) (Figure 6b).
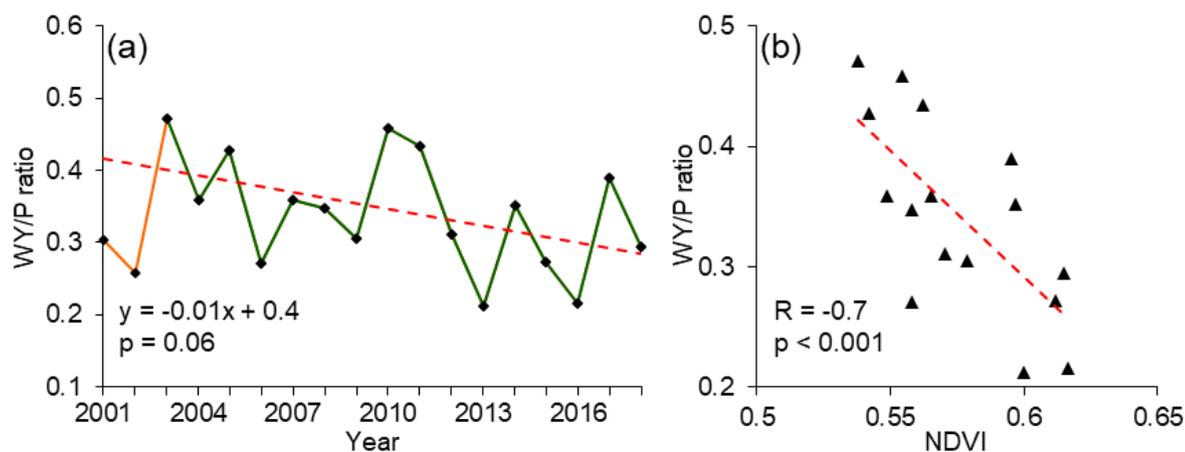
Figure 6: (a) The temporal variation of annual WY/P (water yield/precipitation) ratio during periods before (2001-2003, orange line) and after (2003-2018, green line, the red dotted line denotes the trend for the period 2003-2018) Mann-Kendall change point; (b) The correlation between WY/P ratio and NDVI during 2003-2018.

250

3.4 Potential greening effects on WY in different climate conditions

    The greening trend from 2001 to 2018 significantly reduced WY, but the same greening trend could exert different effects on WY depending on climate conditions (Figure 7). By comparing the WY without greening (Scenario S2) and after greening (Scenario S3) but with dynamic climate variability, we found that the vegetation greening could potentially induce a reduction

255   of 77.1 mm in annual WY on average, accounting for 25% of the mean annual WY (308.5 mm) during 2001-2018. The 2018 vegetation greening condition could have caused the largest decrease in WY by 99.3 mm in 2003 and the least by 43.9 mm in

2001 (Figure 7). The relative changes in WY derived from S2 and S3 during 2001-2018 ranged from 14% (2011) to 31% (2002) (Figure 7).
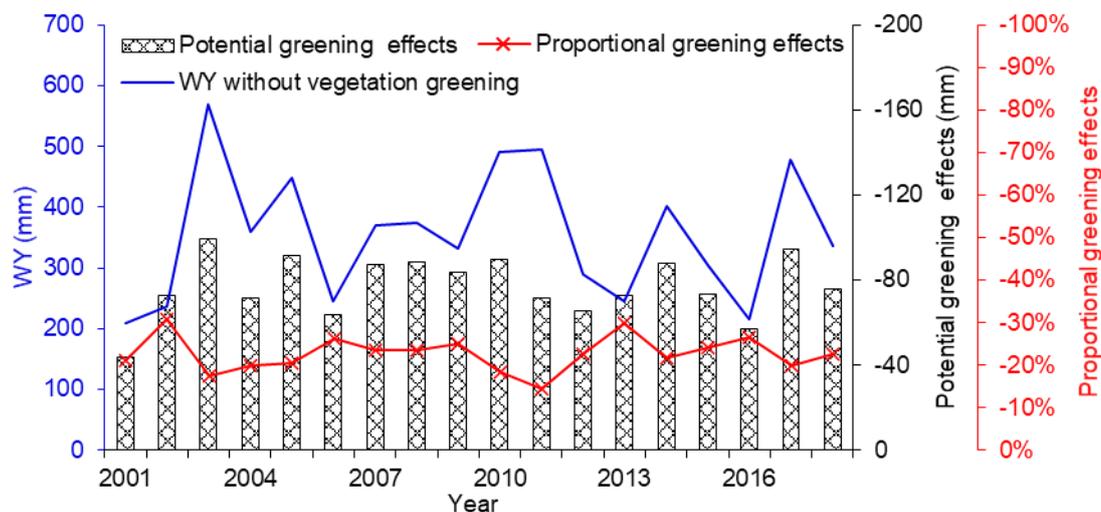
Figure 7: The annual water yield (WY) without vegetation greening and potential effects of vegetation greening on WY from 2001~2018 derived from the difference between S2 and S3 under different climate condition and their proportion to WY without greening.

The differences in potential vegetation greening effects on WY could result from different climate conditions in those years. In order to understand the relationship between the potential greening effects on WY and climate, we explored the correlation between greening-induced ET and WY changes and climate variables (Figure 8). The three climate variables (SR, T, VPD) have strong positive correlations (R > 0.6) with potential absolute ET changes from greening (Figure 8), indicating that vegetation greening would increase ET more in a warmer and drier climate. In contrast, the three climate variables are not as strongly correlated with potential absolute WY changes from greening (Figure 8). The nature of the relationship reversed for potential relative WY changes from greening compared with those of the absolute WY changes. The greening effects on proportional change in WY were positively correlated with T (R = 0.7, p = 0.02), SR (R = 0.5, p = 0.00), and VPD (R = 0.4, p = 0.06) (Figure 8), and negatively correlated with P (R = -0.7, p = 0.00), indicating that vegetation greening could cause more proportional WY decrease in dry years. Regression analyses also revealed that the proportional WY changes from greening would increase one percentage point per 0.1°C increase in T, 0.3 hPa increase in VPD.
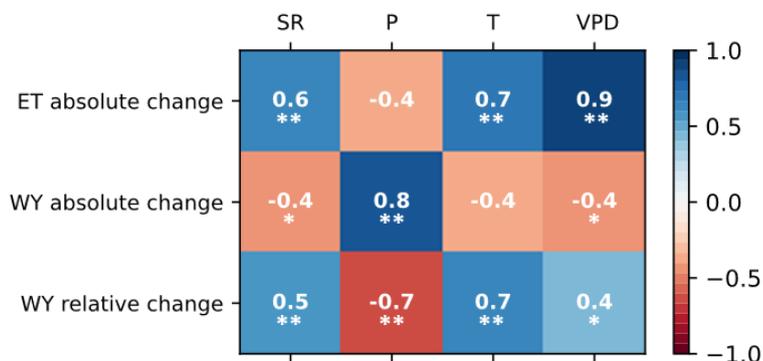
275 **Figure 8: Correlation coefficients between greening induced evapotranspiration (ET) and water yield (WY) changes and climate variables (shortwave radiation, SR; precipitation, P; temperature, T; and vapor pressure deficit, VPD). The absolute changes refer to total magnitude change in ET or WY from vegetation greening, while the relative changes denote the proportional change in WY after greening relative to WY without any greening. The numbers in boxes are the corresponding correlation coefficients. Double asterisks denote p<0.05; single asterisks denote p<0.10.**

280 **3.5 Changes in hydrological drought risk from vegetation greening**

Hydrological drought risks increased due to vegetation greening. There were 109 drought months during 2001-2018 based on scenario S1 (dynamic climate and vegetation), but there were only 87 drought months of the same intensity in the scenario without greening (S2) (Figure 9). In contrast, the number of hydrological drought months increased to 132 in the scenario with 2018 greenness (S3) (Figure 9). The risk of extreme hydrological drought more than doubled between the scenarios without

285 greening (17 total months) and after greening (42 total months), indicating that vegetation greening during 2001-2018 could not only increase the occurrence risks of hydrological drought but could also amplify existing hydrological droughts.

14
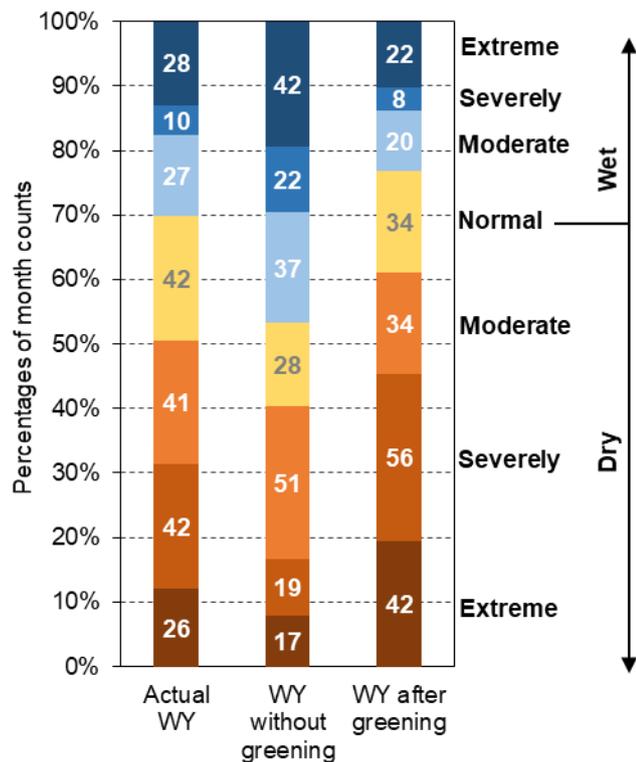
Figure 9: The percentages of counts of months in the different hydrological drought intensities for actual water yield (WY) (S1), WY without greening (S2), WY after greening (S3) (numbers in color bars are the corresponding counts of months).

290   Given that the monsoon period (July-November) contributes about 70% of annual WY in the UHRB, changes in hydrological drought risk during the monsoon period is more critical to water supply capacity to the water diversion project than other months. Nearly two-thirds (63%) of months experiencing severe or extreme hydrological drought for scenario S1 were during the monsoon periods (July-November) of 2001-2018. Vegetation greening could potentially cause a reduction in WY during the monsoon period of 38.2 mm on average, accounting for 18% of the mean WY without greening during the monsoon period.

295   The six driest monsoon periods were in severe or extreme hydrological drought (less than 70% of mean WY) during 2001-2018, during which vegetation greening could potentially cause a WY decrease of 23.2 mm, accounting for 23% of the WY without greening.

4 Discussion

4.1 Reduced water yield and drought amplification from greening

300   The relationship between vegetation and the water cycle is one of the most classic issues in the area of ecohydrology. Many paired catchment and modelling studies provided evidence that vegetation greening and/or afforestation would increase ET and decrease WY (Bosch and Hewlett, 1982; Farley et al., 2005; Liu et al., 2008). However, the extent of the effects of vegetation greening varies in different climate conditions (Bai et al., 2020; Ingwersen, 1985). WY is more sensitive to vegetation greening in water-limited regions than in energy-limited regions (Feng et al., 2016). For example, in the Loess

305   Plateau, an arid/semi-arid area of China, the ratio of annual WY to P decreased from 8% before afforestation (1980-1999) to 5% as vegetation increased during 2000-2010 (Feng et al., 2016). Unlike the Loess Plateau, vegetation greening in the UHRB did not dominate the long-term trend of WY, but climate (especially P) did, which is consistent with previous studies in the subtropical zone (Guo et al., 2008; Hu et al., 2005; Twine et al., 2004). In contrast, the Poyang Lake basin, a subtropical basin in southeast China with an annual P of around 1,800 mm, experienced greening as well, but the ratio of WY to P even increased

310   from 0.38 in 2004 to 0.52 in 2014 based on the observed data, which is attributed to increased soil moisture induced by vegetation greening (Wang et al., 2018).

The UHRB is located on the southern side of the Qinling Mountains, which marks the northern edge of the subtropical monsoon and the dividing line between the subtropical and temperate zones in China (Figure 1a). The P in the UHRB is less than that of other subtropical basins (e.g., Poyang Lake basin), but ET of the UHRB is comparable to those subtropical basins due to

315   the abundance of vegetation. The climate regime and vegetation cover make the UHRB more likely to suffer hydrological drought, and the water cycle can be largely influenced by vegetation dynamics. While the WY of the Poyang Lake basin would only decrease approximately 3% even under an extreme greening scenario (Guo et al., 2008; Tang et al., 2018), the effects of vegetation greening on the water cycle in the UHRB are much larger than this, with a decrease in WY up to 25% for comparable levels of vegetation greening (Figure 5c).

320   Climate is also a critical factor in the interaction between vegetation and the water cycle. Drought risk has increased globally in recent decades and will continue to rise in the future as a result of global warming (Cook et al., 2020; Huang et al., 2016; Lesk et al., 2016; Williams et al., 2020). An increase in temperature directly raises the saturation vapor pressure, which in turn increases global VPD (Yuan et al., 2019; Zhang et al., 2019a), especially when combined with a decrease in oceanic evaporation (Trenberth et al., 2007), which contributes approximately 85% of atmospheric water vapor. Here, we show that

325   the same greening trend could cause more decline in WY under conditions of higher temperature and VPD. Leaf area index in the UHRB is expected to continue increasing in the foreseeable future, even under the Representative Concentration Pathway 2.6 (Mahowald et al., 2016), regardless of whether new forests will be created in the UHRB. Future trends of precipitation in the UHRB are uncertain (Chen and Frauenfeld, 2014; Feng et al., 2011; Guo et al., 2018), but water availability would likely be lower in the UHRB after vegetation greening compared to the same climate conditions but without vegetation greening.

4.2 Reduced capacity of water supply to SNWDP from greening

Since the UHRB was chosen as the source water areas of the middle route of the SNWDP, whether the basin has the capacity to supply enough water to the project is one of the most debated issues about the project (Barnett et al., 2015; Stone, 2006; Zhang et al., 2020). According to a report from the Chinese government (Wang and Yang, 2005), the perennial mean water available for diversion from the UHRB is 12-14 km^3 yr^{-1} and 6.2 km^3 yr^{-1} in dry years. However, severe droughts were not included (Barnett et al., 2015), and increasing drought events will challenge the feasibility of the project (Liu et al., 2015). According to official statistics of the SNWDP (middle route), the capacity of the water supply of the UHRB seems unlikely to meet expectations. The diverted water from the UHRB increased gradually from 2.3 km^3 in 2015 (the first year of the middle route SNWDP operation) to 6.9 km^3 in 2019 but did not reach the maximum designed water diversion volume in Phase I of the project (9.5 km^3) so far. Apart from the project not yet being in full operation, another important reason for the low water diversion rate was the insufficient WY in the UHRB during the operational period relative to long-term levels (Zhang et al., 2020).

The water supply capacity of the UHRB was determined by two factors: 1) the magnitude of WY in the UHRB and 2) the downstream water demand. The inflow of the Danjiangkou Reservoir showed a sharp decrease since 1990, decreasing from 41.0 km^3 during 1951-1989 to 31.6 km^3 yr^{-1} during 1990-2006, largely attributed to P reduction (Liu et al., 2012). We also show that WY for the overall UHRB was likely further reduced to 29.3 km^3 yr^{-1} during 2001-2018. In the future, as the modelling experiments show (e.g., scenario S3), WY could vary within 15.2-44.6 km^3 yr^{-1} (26.5 km^3 yr^{-1} on average) even if vegetation greenness does not continue to increase beyond 2018 levels and the climate regime remains consistent. At the same time, the UHRB must meet the downstream water use demand, including household, agriculture, and industry, as well as maintaining a basic flow rate for shipping and pollutant dilution (Li et al., 2017; Liu et al., 2003). These downstream water demands likely range from 12.2 to 18.5 km^3 yr^{-1} (Hu and Guo, 2006; Li et al., 2017; Liu et al., 2003; Xu and Chang, 2009). The capacity of water supply to the SNWDP can be approximately estimated as WY of UHRB minus the downstream water demand. Therefore, the multi-year average water supply capacity would be only about 14 km^3 yr^{-1} under scenario S3, assuming the low bound downstream water demand (12.2 km^3 yr^{-1}). In contrast, the water supply capacity would be about 21 km^3 yr^{-1} if the UHRB had pre-2001 vegetation conditions, as simulated in scenario S2, which indicated that the vegetation greening during 2001-2018 could decrease the water supply capacity of UHRB to the SNWDP by 7.3 km^3 yr^{-1}, accounting for 77% of the planned annual water diversion target of the Phase I project (9.5 km^3 yr^{-1}). This estimate represents the potential maximum volume of water that can be served to the SNWDP. Under the influence of water abandonment in flooding season and the low diversion rate due to low reservoir water levels in the drought season, the real water supply to the SNWDP could be much lower than this estimate.

The capacity of water supply to the SNWDP at a seasonal scale was highly related to the possibility of hydrological drought in the UHRB. The water supply rate to the project is controlled with a unifying operation principle based on the real-time water level of the Danjiangkou Reservoir. Therefore, the SNWDP can withstand hydrological drought for short periods due to the

17

huge storage capacity of the reservoir, but vegetation greening can significantly increase the risk and duration of hydrological

drought. The water storage of the reservoir would rapidly decrease as hydrological drought progresses, thus directly lowering

365   the water diversion potential to the SNWDP. Moreover, the intensity of the hydrological drought determines the magnitude of

water deficit relative to SNWDP demand. Vegetation greening can also greatly exacerbate existing hydrological drought,

which not only amplifies the water supply deficit to the SNWDP during hydrological drought but can also cause more severe

local water shortages. Overall, our study suggests that afforestation could potentially reduce local WY, thus weakening the

capacity of the water supply to SNWDP.

370   **4.3 Implications for water diversion projects**

Compared to other water diversion projects (WDPs) around the world, the middle route of the SNWDP diverts a much larger

proportion of WY from the source basin (UHRB) (Shumilova et al., 2018). The UHRB serves about one-third to half of the

total WY to the SNWDP. In contrast, 78% of the WDPs in the US in 1973-1982 extracted <1% of annual streamflow from the

source basins (Emanuel et al., 2015). Consequently, the middle route of the SNWDP has more influence on the natural water

375   balance in the water source basin, and the water diversion capacity is more vulnerable to hydrological drought events. In

addition, the downstream of the UHRB has more than 12 million people, 12,000 km^2 of farmland, and large-scale industries

whose water-use demand is an important constraint on water diversion. To stabilize the water supply of the middle route of

the SNWDP, the Phrase II project is currently being planned, which will construct an additional canal to divert water from the

Three Gorges Reservoir in the mainstream Yangtze River to the Danjiangkou Reservoir. After the Phase II project is completed,

380   the UHRB will not be the only source for diverted water, and the water supply to the SNWDP will be more stable. However,

the additional engineering exerts more human influence on the water cycle, and its unintended consequences for hydrological

and environmental systems remain uncertain.

China has 59 major WDPs, each with a total canal length of at least 50 km or an annual water diversion volume greater than

0.1 km^3 (Yu et al., 2018). Watershed protection measures such as large-scale afforestation have been implemented for more

385   than twenty years in China. Afforestation and ecological restoration in water source basins of WDPs can help control sediment

and thus improve water quality, but vegetation greening can also cause negative effects on water availability, thus lowering

the operational effectiveness of WDPs. Rapid vegetation greening occurred in most of China in recent decades, which is

projected to continue in the foreseeable future (Liu et al., 2015). Therefore, navigating this tradeoff between water quality

improvement and water resource availability should be an important consideration for current and future WDPs.

390   Managing water stress needs to consider both supply and demand. From the perspective of water demand (North China), the

water transferred from the south supplied more than 70% of the domestic water use in the project-served cities in 2019.

Moreover, the probability of concurrent drought events between the UHRB and North China is highly likely to increase in the

next 30 years (Liu et al., 2015). Consequently, any fluctuation of WY in the water source region (the UHRB) or any problem

with project facilities would influence the water supply of the serviced cities with a huge population. Therefore, it is risky for

Hydrology and
Earth System
Sciences
Discussions

Open Access

EGU

395 North China cities to become over-dependent on water diversion and comprehensive water management policies are needed to sustain the water supply from the UHRB basin while meeting the water demand in North China.

5 Conclusions

Using a new watershed ecohydrological model, we found that vegetation greening in the Upper Han River Basin (UHRB) greatly decreased both annual water yield (WY) and the ratio of WY to precipitation over the study period (2001-2018),

400 potentially reducing the annual capacity of water supply to the South to North Water Diversion Projects (SNWDP). Vegetation greening could also exacerbate hydrological drought risk and reduce about a quarter of WY on average during hydrological drought periods. In the future, hydrological drought risk will likely continue to increase in the UHRB due to increases in temperature and vapor pressure deficit, which could be compounded by increasing vegetation greenness and may seriously reduce the water availability for the middle route of the SNWDP. Our study suggests that improved watershed management

405 (e.g., forest management and reducing water use) is needed to address the effects of vegetation greening and climate change on water supply capacity in watersheds serving as water sources for large water diversion projects.

Author contributions. J. Z developed the model code, did the simulation experiments, wrote the paper and made tables and figures; Y. Z. and G. S. and C. S. provided ideas, edited the manuscript, gave constructive suggestions; M. P. D. edited the

410 manuscript, gave constructive suggestions; J. L. gave constructive suggestions; N. L. provided codes for data processing; K. Z. and Q. Z. provided the streamflow data for model evaluation.

Competing interests. The authors declare that they have no conflict of interest.

Code and data availability. Data sets used for driving model were obtained from different sources described in the Table 1. The monthly streamflow records of six hydrological gauging stations for model evaluation were derived from Yearbook of the

415 Han River Hydrology. The inflow records of Danjiangkou Reservoir were derived from http://113.57.190.228:8001/web/Report/BigMSKReport#. All the data related to our results in this study can be found at https://osf.io/f5bgk/, except the monthly streamflow records for six hydrological gauging stations are available upon reasonable requests.

References

Abatzoglou, J. T., Dobrowski, S. Z., Parks, S. A. and Hegewisch, K. C.: TerraClimate, a high-resolution global dataset of monthly climate and climatic water balance from 1958-2015, Scientific Data, 5(1), 170191, https://doi.org/10.1038/sdata.2017.191, 2018.

Bai, Shen, Song, Mo, Huang and Quan: Multi-Temporal Variabilities of Evapotranspiration Rates and Their Associations with Climate Change and Vegetation Greening in the Gan River Basin, China, Water, 11(12), 2568, https://doi.org/10.3390/w11122568, 2019.

Bai, P., Liu, X., Zhang, Y. and Liu, C.: Assessing the impacts of vegetation greenness change on evapotranspiration and water yield in China, Water Resources Research, 0–2, https://doi.org/10.1029/2019WR027019, 2020.

Baker, T. J. and Miller, S. N.: Using the Soil and Water Assessment Tool (SWAT) to assess land use impact on water resources in an East African watershed, Journal of Hydrology, 486, 100–111, https://doi.org/10.1016/j.jhydrol.2013.01.041, 2013.

Barnett, J., Rogers, S., Webber, M., Finlayson, B. and Wang, M.: Sustainability: Transfer project cannot meet China's water needs, Nature, 527(7578), https://doi.org/10.1038/527295a, 2015.

Bosch, J. M. and Hewlett, J. D.: A review of catchment experiments to determine the effect of vegetation changes on water yield and evapotranspiration, Journal of Hydrology, 55(1–4), 3–23, https://doi.org/10.1016/0022-1694(82)90117-2, 1982.

Burnash, R.: The NWS river forecast system-catchment modeling, Computer models of watershed hydrology, 311–366, 1995.

Burnash, R., Ferral, L. and McGuire, R.: A generalized streamflow simulation system: Conceptual modeling for digital computers, US Department of Commerce, National Weather Service, and State of California~…., 1973.

Caldwell, P. v, Sun, G., Mcnulty, S. G., Cohen, E. C. and Myers, J. A. M.: Impacts of impervious cover, water withdrawals, and climate change on river flows in the conterminous US, Hydrol. Earth Syst. Sci, 16, 2839–2857, https://doi.org/10.5194/hess-16-2839-2012, 2012.

Cao, S., Zhang, J., Chen, L. and Zhao, T.: Ecosystem water imbalances created during ecological restoration by afforestation in China, and lessons for other developing countries, Journal of Environmental Management, 183, 843–849, https://doi.org/10.1016/j.jenvman.2016.07.096, 2016.

Chen, C., Park, T., Wang, X., Piao, S., Xu, B., Chaturvedi, R. K., Fuchs, R., Brovkin, V., Ciais, P., Fensholt, R., Tømmervik, H., Bala, G., Zhu, Z., Nemani, R. R. and Myneni, R. B.: China and India lead in greening of the world through land-use management, Nature Sustainability, 2(2), 122–129, https://doi.org/10.1038/s41893-019-0220-7, 2019.

Chen, H., Guo, S., Xu, C. and Singh, V. P.: Historical temporal trends of hydro-climatic variables and runoff response to climate variability and their relevance in water resource management in the Hanjiang basin, Journal of Hydrology, 344(3–4), 171–184, https://doi.org/10.1016/j.jhydrol.2007.06.034, 2007.

Chen, L. and Frauenfeld, O. W.: A comprehensive evaluation of precipitation simulations over China based on CMIP5 multimodel ensemble projections, Journal of Geophysical Research, 119(10), 5767–5786, https://doi.org/10.1002/2013JD021190, 2014.

455   China Meteorological Administration: Yearbook of Meteorological Disasters in China, Beijing., 2019.

Cook, B. I., Smerdon, J. E., Seager, R. and Coats, S.: Global warming and 21st century drying, Climate Dynamics, 43(9–10), 2607–2627, https://doi.org/10.1007/s00382-014-2075-y, 2014.

Cook, B. I., Mankin, J. S., Marvel, K., Williams, A. P., Smerdon, J. E. and Anchukaitis, K. J.: Twenty-First Century Drought Projections in the CMIP6 Forcing Scenarios, Earth's Future, 8(6), https://doi.org/10.1029/2019EF001461, 2020.

460   Emanuel, R. E., Buckley, J. J., Caldwell, P. v., McNulty, S. G. and Sun, G.: Influence of basin characteristics on the effectiveness and downstream reach of interbasin water transfers: Displacing a problem, Environmental Research Letters, 10(12), 124005, https://doi.org/10.1088/1748-9326/10/12/124005, 2015.

Farley, K. A., Jobbágy, E. G. and Jackson, R. B.: Effects of afforestation on water yield: A global synthesis with implications for policy, Global Change Biology, 11(10), 1565–1576, https://doi.org/10.1111/j.1365-2486.2005.01011.x, 2005.

465   Feng, L., Zhou, T., Wu, B., Li, T. and Luo, J.-J.: Projection of future precipitation change over China with a high-resolution global atmospheric model, Advances in Atmospheric Sciences, 28(2), https://doi.org/10.1007/s00376-010-0016-1, 2011.

Feng, X., Fu, B., Piao, S., Wang, S., Ciais, P., Zeng, Z., Lü, Y., Zeng, Y., Li, Y., Jiang, X. and Wu, B.: Revegetation in China's Loess Plateau is approaching sustainable water resource limits, Nature Climate Change, 6(11), 1019–1022, https://doi.org/10.1038/nclimate3092, 2016.

470   Guo, H., Hu, Q. and Jiang, T.: Annual and seasonal streamflow responses to climate and land-cover changes in the Poyang Lake basin, China, Journal of Hydrology, 355(1–4), 106–122, https://doi.org/10.1016/j.jhydrol.2008.03.020, 2008.

Guo, J., Huang, G., Wang, X., Li, Y. and Yang, L.: Future changes in precipitation extremes over China projected by a regional climate model ensemble, Atmospheric Environment, 188, 142–156, https://doi.org/10.1016/j.atmosenv.2018.06.026, 2018.

Hamed, K. H.: Trend detection in hydrologic data: The Mann-Kendall trend test under the scaling hypothesis, Journal of
475   Hydrology, 349(3–4), 350–363, https://doi.org/10.1016/j.jhydrol.2007.11.009, 2008.

Hayes, M. J., Alvord, C. and Lowrey, J.: Drought indices, National Drought Mitigation Center, University of Nebraska., 2002.

Hu, A. Y. and Guo, H. J.: Discussion on ecological environment water demand in the middle-lower reaches of Han River river, China Water Resources (in Chinese), (23), 14–16, 2006.

Huang, J., Yu, H., Guan, X., Wang, G. and Guo, R.: Accelerated dryland expansion under climate change, Nature Climate
480   Change, 6(2), 166–171, https://doi.org/10.1038/nclimate2837, 2016.

Huete, A., Didan, K., Miura, T., Rodriguez, E. P., Gao, X. and Ferreira, L. G.: Overview of the radiometric and biophysical performance of the MODIS vegetation indices, Remote Sensing of Environment, 83(1–2), 195–213, https://doi.org/10.1016/S0034-4257(02)00096-2, 2002.

Ingwersen, J. B.: Fog drip, water yield, and timber harvesting in the bull run municipal watershed, Oregon, Journal of the
485   American Water Resources Association, 21(3), 469–473, https://doi.org/10.1111/j.1752-1688.1985.tb00158.x, 1985.

Jackson, R. B., Carpenter, S. R., Dahm, C. N., McKnight, D. M., Naiman, R. J., Postel, S. L. and Running, S. W.: Water in a changing world, Ecological Applications, 11(4), 1027–1045, https://doi.org/10.1890/1051-0761(2001)011[1027:WIACW]2.0.CO;2, 2001.

Jackson, R. B., Jobbágy, E. G., Avissar, R., Roy, S. B., Barrett, D. J., Cook, C. W., Farley, K. A., le Maitre, D. C., McCarl, B.
490   A. and Murray, B. C.: Atmospheric science: Trading water for carbon with biological carbon sequestration, Science, 310(5756), 1944–1947, https://doi.org/10.1126/science.1119282, 2005.

Jin, R. and Guo, H.: Water resources assessment in the water source areas of the Middle Route of the South to North Water Transfer Project and water quantity analysis in the Danjiangkou Reservoir, Yangzte River, 24(11), 7–12, 1993.

Jönsson, P. and Eklundh, L.: TIMESAT - A program for analyzing time-series of satellite sensor data, Computers and
495   Geosciences, 30(8), 833–845, https://doi.org/10.1016/j.cageo.2004.05.006, 2004.

Lesk, C., Rowhani, P. and Ramankutty, N.: Influence of extreme weather disasters on global crop production, Nature, 529(7584), 84–87, https://doi.org/10.1038/nature16467, 2016.

Li, S., Gu, S., Liu, W., Han, H. and Zhang, Q.: Water quality in relation to land use and land cover in the upper Han River Basin, China, CATENA, 75(2), 216–222, https://doi.org/10.1016/J.CATENA.2008.06.005, 2008.

500   Li, Y., Cui, Q., Li, C., Wang, X., Cai, Y., Cui, G. and Yang, Z.: An improved multi-objective optimization model for supporting reservoir operation of China's South-to-North Water Diversion Project, Science of The Total Environment, 575, 970–981, https://doi.org/10.1016/j.scitotenv.2016.09.165, 2017.

Li, Y., Piao, S., Li, L. Z. X., Chen, A., Wang, X., Ciais, P., Huang, L., Lian, X., Peng, S., Zeng, Z., Wang, K. and Zhou, L.: Divergent hydrological response to large-scale afforestation and vegetation greening in China, Science Advances, 4(5),
505   eaar4182, https://doi.org/10.1126/sciadv.aar4182, 2018.

Liu, B. J., Shao, D. G., Xu, M. X. and Yang, S. M.: Research of the water resources utilization relationship between the middle route of South-to North Water Transfer Project and the middle and lower Basin of Hanjiang River, South-to-North Water Transfers and Water Science and Technology (in Chinese), 1(6), 6–9, 2003.

Liu, C. and Zheng, H.: South-to-north water transfer schemes for China, International Journal of Water Resources
510   Development, 18(3), 453–471, https://doi.org/10.1080/0790062022000006934, 2002.

Liu, M., Tian, H., Chen, G., Ren, W., Zhang, C. and Liu, J.: Effects of Land-Use and Land-Cover Change on Evapotranspiration and Water Yield in China During 1900-2000, JAWRA Journal of the American Water Resources Association, 44(5), 1193–1207, https://doi.org/10.1111/j.1752-1688.2008.00243.x, 2008.

Liu, N., Sun, P., Caldwell, P. v., Harper, R., Liu, S. and Sun, G.: Trade-off between watershed water yield and ecosystem
515   productivity along elevation gradients on a complex terrain in southwestern China, Journal of Hydrology, 125449, https://doi.org/10.1016/j.jhydrol.2020.125449, 2020.

Liu, X., Liu, C., Luo, Y., Zhang, M. and Xia, J.: Dramatic decrease in streamflow from the headwater source in the central route of China's water diversion project: Climatic variation or human influence?, Journal of Geophysical Research: Atmospheres, 117(D6), n/a-n/a, https://doi.org/10.1029/2011JD016879, 2012.

520 Liu, X., Luo, Y., Yang, T., Liang, K., Zhang, M. and Liu, C.: Investigation of the probability of concurrent drought events between the water source and destination regions of China's water diversion project, Geophysical Research Letters, 42(20), 8424–8431, https://doi.org/10.1002/2015GL065904, 2015.

van Loon, A. F.: Hydrological drought explained, Wiley Interdisciplinary Reviews: Water, 2(4), 359–392, https://doi.org/10.1002/wat2.1085, 2015.

525 van Loon, A. F., Gleeson, T., Clark, J., van Dijk, A. I. J. M., Stahl, K., Hannaford, J., di Baldassarre, G., Teuling, A. J., Tallaksen, L. M., Uijlenhoet, R., Hannah, D. M., Sheffield, J., Svoboda, M., Verbeiren, B., Wagener, T., Rangecroft, S., Wanders, N. and van Lanen, H. A. J.: Drought in the Anthropocene, Nature Geoscience, 9(2), 89–91, https://doi.org/10.1038/ngeo2646, 2016.

Mahowald, N., Lo, F., Zheng, Y., Harrison, L., Funk, C., Lombardozzi, D. and Goodale, C.: Projections of leaf area index in 530 earth system models, Earth System Dynamics, 7(1), 211–229, https://doi.org/10.5194/esd-7-211-2016, 2016.

McCuen, R. H., Knight, Z. and Cutter, A. G.: Evaluation of the Nash–Sutcliffe Efficiency Index, Journal of Hydrologic Engineering, 11(6), 597–602, https://doi.org/10.1061/(asce)1084-0699(2006)11:6(597), 2006.

Pastorello, G., Trotta, C., Canfora, E., Chu, H., Christianson, D., Cheah, Y. W., Poindexter, C., Chen, J., Elbashandy, A., Humphrey, M., Isaac, P., Polidori, D., Ribeca, A., van Ingen, C., Zhang, L., Amiro, B., Ammann, C., Arain, M. A., Ardö, J., 535 Arkebauer, T., Arndt, S. K., Arriga, N., Aubinet, M., Aurela, M., Baldocchi, D., Barr, A., Beamesderfer, E., Marchesini, L. B., Bergeron, O., Beringer, J., Bernhofer, C., Berveiller, D., Billesbach, D., Black, T. A., Blanken, P. D., Bohrer, G., Boike, J., Bolstad, P. v., Bonal, D., Bonnefond, J. M., Bowling, D. R., Bracho, R., Brodeur, J., Brümmer, C., Buchmann, N., Burban, B., Burns, S. P., Buysse, P., Cale, P., Cavagna, M., Cellier, P., Chen, S., Chini, I., Christensen, T. R., Cleverly, J., Collalti, A., Consalvo, C., Cook, B. D., Cook, D., Coursolle, C., Cremonese, E., Curtis, P. S., D'Andrea, E., da Rocha, H., Dai, X., Davis, 540 K. J., de Cinti, B., de Grandcourt, A., de Ligne, A., de Oliveira, R. C., Delpierre, N., Desai, A. R., di Bella, C. M., di Tommasi, P., Dolman, H., Domingo, F., Dong, G., Dore, S., Duce, P., Dufrêne, E., Dunn, A., Dušek, J., Eamus, D., Eichelmann, U., ElKhidir, H. A. M., Eugster, W., Ewenz, C. M., Ewers, B., Famulari, D., Fares, S., Feigenwinter, I., Feitz, A., Fensholt, R., Filippa, G., Fischer, M., Frank, J., Galvagno, M., Gharun, M., Gianelle, D., et al.: The FLUXNET2015 dataset and the ONEFlux processing pipeline for eddy covariance data, Scientific data, 7(1), 225, https://doi.org/10.1038/s41597-020-0534-545 3, 2020.

Piégay, H., Walling, D. E., Landon, N., He, Q., Liébault, F. and Petiot, R.: Contemporary changes in sediment yield in an alpine mountain basin due to afforestation (the upper Drôme in France), Catena, 55(2), 183–212, 2004.

She, D., Xia, J., Shao, Q., Taylor, J. A., Zhang, L., Zhang, X., Zhang, Y. and Gu, H.: Advanced investigation on the change in the streamflow into the water source of the middle route of China's water diversion project, Journal of Geophysical Research: Atmospheres, 122(13), 6950–6961, https://doi.org/10.1002/2016JD025702, 2017.

Shin, H., Park, M., Lee, J., Lim, H. and Kim, S. J.: Evaluation of the effects of climate change on forest watershed hydroecology using the RHESSys model: Seolmacheon catchment, Paddy and Water Environment, 17(4), 581–595, https://doi.org/10.1007/s10333-018-00683-1, 2019.

Shumilova, O., Tockner, K., Thieme, M., Koska, A. and Zarfl, C.: Global Water Transfer Megaprojects: A Potential Solution for the Water-Food-Energy Nexus?, Frontiers in Environmental Science, 6(DEC), 150, https://doi.org/10.3389/fenvs.2018.00150, 2018.

Soutar, R. G.: Afforestation and sediment yields in British fresh waters, Soil Use and Management, 5(2), 82–86, 1989.

Stone, R.: Hydroengineering: Going Against the Flow, Science, 313(5790), https://doi.org/10.1126/science.313.5790.1034, 2006.

Sulla-Menashe, D., Gray, J. M., Abercrombie, S. P. and Friedl, M. A.: Hierarchical mapping of annual global land cover 2001 to present: The MODIS Collection 6 Land Cover product, Remote Sensing of Environment, 222, 183–194, https://doi.org/10.1016/j.rse.2018.12.013, 2019.

Sun, G., Caldwell, P., Noormets, A., McNulty, S. G., Cohen, E., Moore Myers, J., Domec, J.-C., Treasure, E., Mu, Q., Xiao, J., John, R. and Chen, J.: Upscaling key ecosystem functions across the conterminous United States by a water-centric ecosystem model, Journal of Geophysical Research, 116, G00J05, https://doi.org/10.1029/2010JG001573, 2011.

Sun, G., Domec, J.-C., Amatya, D. M. and others: Forest evapotranspiration: measurements and modeling at multiple scales, Forest Hydrology: Processes, Management and Assessment, 19, 32–50, 2016.

Sun, S., Sun, G., Caldwell, P., McNulty, S., Cohen, E., Xiao, J. and Zhang, Y.: Drought impacts on ecosystem functions of the U.S. National Forests and Grasslands: Part II assessment results and management implications, Forest Ecology and Management, 353, 269–279, https://doi.org/10.1016/j.foreco.2015.04.002, 2015.

Tang, L.-L., Cai, X.-B., Gong, W.-S., Lu, J.-Z., Chen, X.-L., Lei, Q. and Yu, G.-L.: Increased Vegetation Greenness Aggravates Water Conflicts during Lasting and Intensifying Drought in the Poyang Lake Watershed, China, Forests, 9(1), 24, https://doi.org/10.3390/f9010024, 2018.

Teuling, A. J., van Loon, A. F., Seneviratne, S. I., Lehner, I., Aubinet, M., Heinesch, B., Bernhofer, C., Grünwald, T., Prasse, H. and Spank, U.: Evapotranspiration amplifies European summer drought, Geophysical Research Letters, 40(10), 2071–2075, https://doi.org/10.1002/grl.50495, 2013.

Tian, L., Jin, J., Wu, P. and Niu, G. Y.: Quantifying the impact of climate change and human activities on streamflow in a Semi-Arid Watershed with the Budyko Equation incorporating dynamic vegetation information, Water (Switzerland), 10(12), https://doi.org/10.3390/w10121781, 2018.

580 Trenberth, K. E., Smith, L., Qian, T., Dai, A. and Fasullo, J.: Estimates of the global water budget and its annual cycle using observational and model Data, Journal of Hydrometeorology, 8(4), 758–769, https://doi.org/10.1175/JHM600.1, 2007.

Wang, K. and Dickinson, R. E.: A review of global terrestrial evapotranspiration: Observation, modeling, climatology, and climatic variability, Reviews of Geophysics, 50(2), https://doi.org/10.1029/2011RG000373, 2012.

Wang, Y. and Yang, Y.: South-North Water Transfer Project of China, Yangtze River (in Chinese), 7, 2–5, 2005.

585 Wang, Y., Liu, Y. and Jin, J.: Contrast Effects of Vegetation Cover Change on Evapotranspiration during a Revegetation Period in the Poyang Lake Basin, China, Forests, 9(4), 217, https://doi.org/10.3390/f9040217, 2018.

Wei, X., Sun, G., Liu, S., Jiang, H., Zhou, G. and Dai, L.: The Forest-Streamflow Relationship in China: A 40-Year Retrospect 1, JAWRA Journal of the American Water Resources Association, 44(5), 1076–1085, https://doi.org/10.1111/j.1752-1688.2008.00237.x, 2008.

590 Williams, A. P., Cook, E. R., Smerdon, J. E., Cook, B. I., Abatzoglou, J. T., Bolles, K., Baek, S. H., Badger, A. M. and Livneh, B.: Large contribution from anthropogenic warming to an emerging North American megadrought, Science, 368(6488), 314–318, https://doi.org/10.1126/science.aaz9600, 2020.

Xi, Y., Peng, S., Ciais, P., Guimberteau, M., Li, Y., Piao, S., Wang, X., Polcher, J., Yu, J., Zhang, X., Zhou, F., Bo, Y., Ottle, C. and Yin, Z.: Contributions of Climate Change, CO2, Land-Use Change, and Human Activities to Changes in River Flow
595 across 10 Chinese Basins, Journal of Hydrometeorology, 19(11), https://doi.org/10.1175/JHM-D-18-0005.1, 2018.

Xu, Y. and Chang, F. X.: Preliminary study on requirement rate of ecological water demand in middle and lower reaches of Hanjiang River, Yangtze River Scientific Research Institute (in Chinese), 26(1), 1–4, 2009.

Xu, Y., Lin, S., Huang, Y., Zhang, Q. and Ran, Q.: Drought analysis using multi-scale standardized precipitation index in the Han River Basin, China, Journal of Zhejiang University: Science A, 12(6), 483–494, https://doi.org/10.1631/jzus.A1000450,
600 2011.

Yang, Y., Zhou, N., Guo, X. and Hu, Q.: The hydrology characteristics analysis of HanJiang up-streams, Hydrology, 2(21), 54–56, 1997.

Yu, M., Wang, C., Liu, Y., Olsson, G. and Wang, C.: Sustainability of mega water diversion projects: Experience and lessons from China, Science of the Total Environment, 619–620, 721–731, https://doi.org/10.1016/j.scitotenv.2017.11.006, 2018.

605 Yuan, W., Zheng, Y., Piao, S., Ciais, P., Lombardozzi, D., Wang, Y., Ryu, Y., Chen, G., Dong, W., Hu, Z., Jain, A. K., Jiang, C., Kato, E., Li, S., Lienert, S., Liu, S., Nabel, J. E. M. S., Qin, Z., Quine, T., Sitch, S., Smith, W. K., Wang, F., Wu, C., Xiao, Z. and Yang, S.: Increased atmospheric vapor pressure deficit reduces global vegetation growth, Science Advances, 5(8), eaax1396, https://doi.org/10.1126/sciadv.aax1396, 2019.

Zhang, C., Duan, Q., Yeh, P. J. -F., Pan, Y., Gong, H., Gong, W., Di, Z., Lei, X., Liao, W., Huang, Z., Zheng, L. and Guo, X.:
610 The Effectiveness of the South-to-North Water Diversion Middle Route Project on Water Delivery and Groundwater Recovery in North China Plain, Water Resources Research, 56(10), https://doi.org/10.1029/2019WR026759, 2020.

Zhang, D., Zhang, Q., Qiu, J., Bai, P., Liang, K. and Li, X.: Intensification of hydrological drought due to human activity in the middle reaches of the Yangtze River, China, Science of the Total Environment, 637–638, 1432–1442, https://doi.org/10.1016/j.scitotenv.2018.05.121, 2018.

615   Zhang, Q.: The South-to-North Water Transfer Project of China: Environmental Implications and Monitoring Strategy, JAWRA Journal of the American Water Resources Association, 45(5), 1238–1247, https://doi.org/10.1111/j.1752-1688.2009.00357.x, 2009.

Zhang, Q., Ficklin, D. L., Manzoni, S., Wang, L., Way, D., Phillips, R. P. and Novick, K. A.: Response of ecosystem intrinsic water use efficiency and gross primary productivity to rising vapor pressure deficit, Environmental Research Letters, 14(7),

620   https://doi.org/10.1088/1748-9326/ab2603, 2019a.

Zhang, Y., Song, C., Sun, G., Band, L. E., McNulty, S., Noormets, A., Zhang, Q. and Zhang, Z.: Development of a coupled carbon and water model for estimating global gross primary productivity and evapotranspiration based on eddy flux and remote sensing data, Agricultural and Forest Meteorology, 223, 116–131, https://doi.org/10.1016/j.agrformet.2016.04.003, 2016.

Zhang, Y., Song, C., Band, L. E. and Sun, G.: No Proportional Increase of Terrestrial Gross Carbon Sequestration From the

625   Greening Earth, Journal of Geophysical Research: Biogeosciences, 124(8), 2540–2553, https://doi.org/10.1029/2018jg004917, 2019b.

Zhou, S., Yu, B., Huang, Y. and Wang, G.: The effect of vapor pressure deficit on water use efficiency at the subdaily time scale, Geophysical Research Letters, 41(14), 5005–5013, https://doi.org/10.1002/2014GL060741, 2014.

Hydrology and
Earth System
Sciences
Discussions

Open Access

EGU

630

Appendix A:
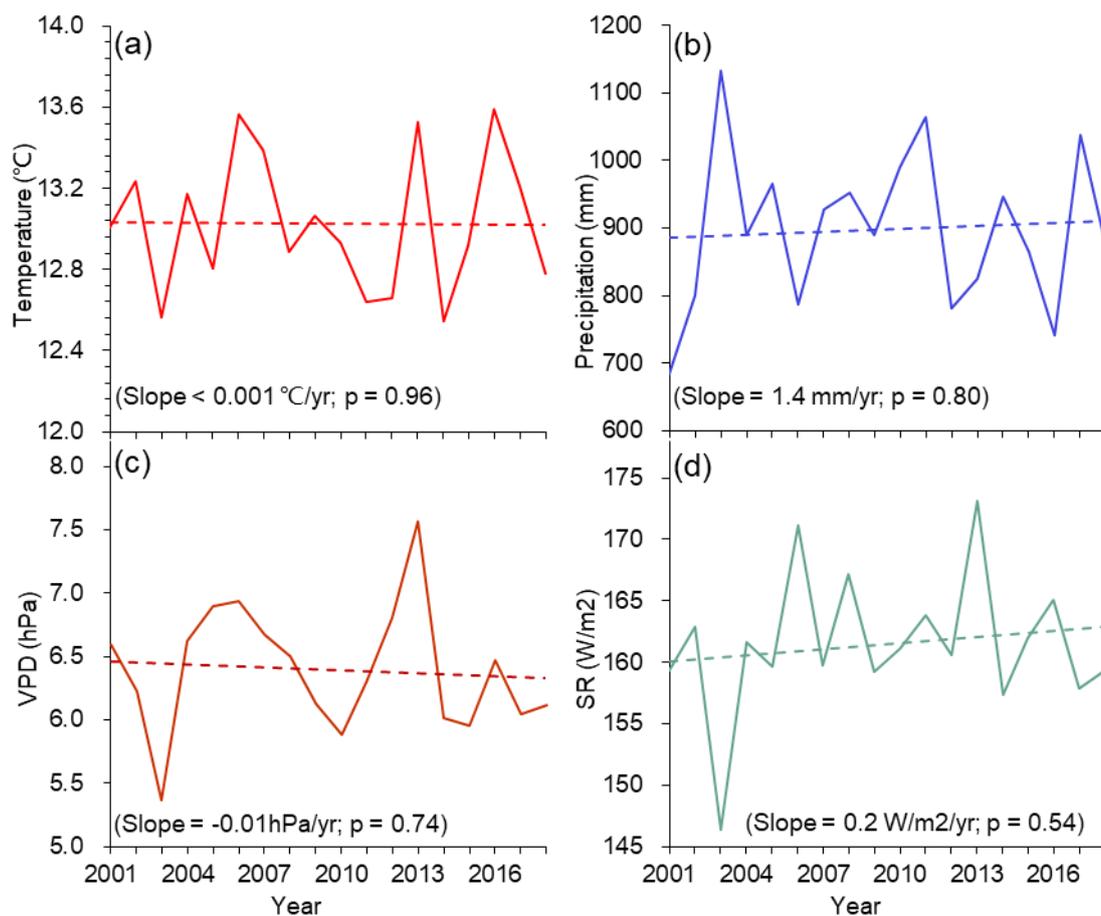
Figure A1. Inter-annual variations of averaged air temperature (a), total precipitation (b), vapor pressure deficit (VPD) (c) and shortwave radiation (SR) (d) in the Upper Han River Basin from 2001 to 2018.
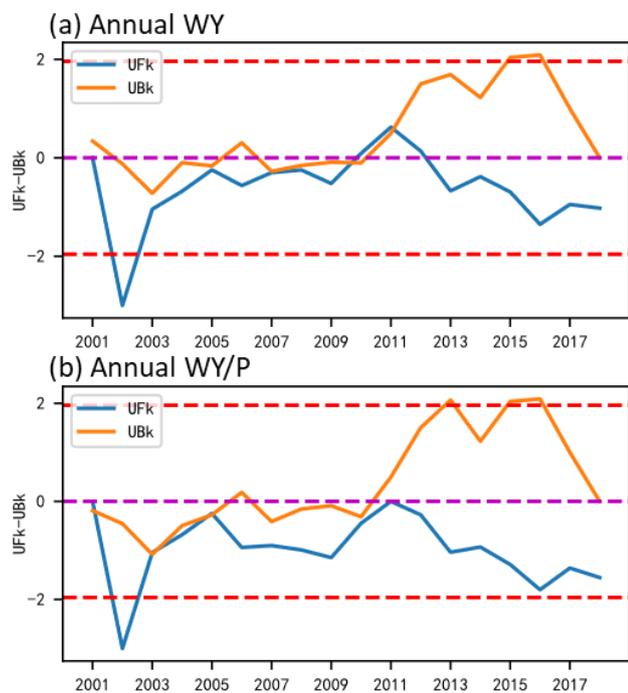
635

Figure A2. Abrupt change detections of the Mann-Kendall for annual water yield (WY) (a) and the ratio between WY and precipitation ratio (b) in the Upper Han River Basin from 2001 to 2018. UBk and UFk are time statistics of the Mann-Kendall method.
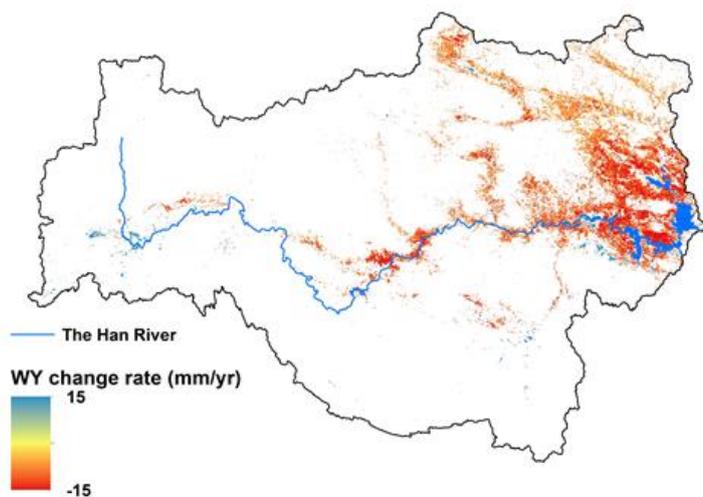
640 **Figure A3. The linear trend of annual water yield (WY) at the confidence level of 90% (p < 0.10).**

28